โครงการ

การเรียนการสอนเพื่อเสริมประสบการณ์

ชื่อโครงการ Simulation of Proton and Photon Depth Dose Distributions using FLUKA and PHITS

ชื่อนิสิต นาสาววริศรา จารุจินดา **เลขประจำตัว** 5833436623

ภาควิชา ฟิสิกส์

ปีการศึกษา 2561

คณะวิทยาศาสตร์ จุฬาลงกรณ์มหาวิทยาลัย

Simulation of Proton and Photon Depth Dose Distributions using FLUKA and PHITS

Warisara Charuchinda

Department of Physics, Faculty of Science

Chulalongkorn University

Submitted in part fulfilment of the requirement for 2304499 Senior Project

Second Semester, Academic Year 2018

Abstract

The most popular radiation therapy currently used for cancer treatment is photon radiation. Nevertheless, there is damage to normal tissue resulting from photon energy deposition. Proton therapy is an alternative radiation therapy currently being used in many countries due to its special depth dose distribution characteristic. In this study, the effects of beam parameters, i.e. initial energy and beam intensity, on the depth dose distribution of photon and proton were determined by using Monte Carlo simulations called PHITS and FLUKA. We also varied the medium which photon and proton projected into, i.e. water, soft tissue, and compact bone. The results show that when beam energy increases, the dose of photon also increases, while the dose of proton decreases. Furthermore, the doses of both photon and proton depend on the beam intensity and the type of media. Soft tissue gives similar results to water but different from compact bone due to the effects of their densities and compositions. We also modified the proton beam to cover the target region. In this study, we assume the target located at 6 - 8 cm from the surface of water. By modulating the peaks appropriately, the extent of the high-dose region can be widened to cover the target region together with a uniform dose. This modulated peak is called spread-out Bragg peak (SOBP). To obtain the SOBP from various mono-energetic beams, the dependences of beam energy and intensity on depth dose distribution mentioned previously were used to calculate the depth dose distribution of mono-energetic beams instead of using PHITS or FLUKA. To generate SOBP to cover this target region, the results show that the energies of the modulated beams at 87.59 - 103.25 MeV are required. The weighted intensities are 0.13 – 0.44 for the modulation of 4 beams and 0.03 – 0.38 for 10 beams.

Acknowledgements

I would like to express my deep gratitude to Assistant Professor Dr. Narumon Suwonjandee and Assistant Professor Dr. Burin Asavapibhob, my supervisors for giving me an opportunity to make an interesting project and for giving me helpful suggestions for doing and writing research. I also would like to express my gratitude for their kind advice which can be used in work-life situation and change my attitude in many ways.

This research is funded by the Development and Promotion of Science and Technology Talents Project (DPST), Chulalongkorn University; Government Budget, and "CUniverse" research promotion project by Chulalongkorn University (grant reference CUAASC).

My grateful thanks are extended to Associate Professor Dr. Nakorn Phaisangittisakul for being my chairman and for willingly giving me knowledge which I can use in my project. They are also extended to Assistant Professor Panadda Dechadilok for being my project committee and for giving comments and suggestions to help me in gaining a deep understanding of my work.

I also would like to give special thanks to the members of Particle Physics Research Laboratory, Dr. Chayanit Asawatangtrakuldee, Dr. Noraphat Srimanobhas, Mr. Jittapan Ineead, Mr. Narongkiat Rodphai and Mr. Nanthanon Visitpongaree which always gave me suggestions and encouragement.

Lastly, I am grateful for my family who always support me in everything I want to do. They give me many advices both for my work and everyday life and deliver warm happiness to me in tough days. These remind me that lots of their encouragement and love is the key to my success.

Warisara Charuchinda

Content

List of Figures

List of Tables

Chapter 1

Introduction

Cancer is the second leading cause of death globally, therefore therapeutic technique development is actively studied. Currently, there are three methods for curing cancer that are surgery, chemotherapy and radiation therapy. Radiation therapy has been developed constantly using physics knowledge. The most popular radiation therapy currently used for cancer treatment is x-ray (photon radiation). Nevertheless, there is damage resulting from energy deposition to healthy tissue. In Fig. 1.1, the amount of radiation of photon radiation and proton radiation in brain tissue are compared.

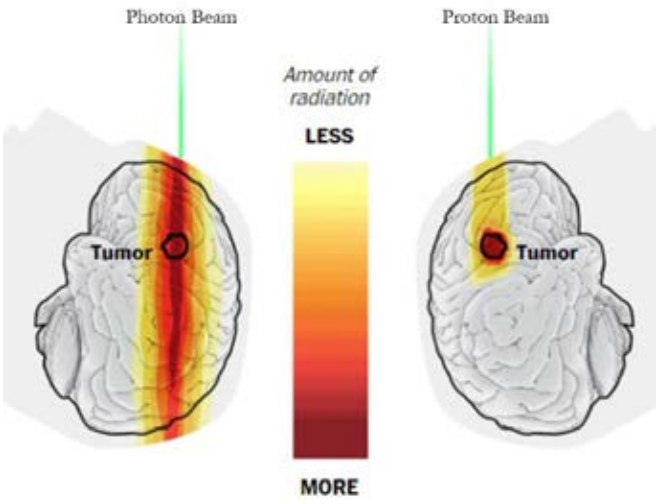

Fig. 1.1 Comparison between amount of radiation of photon radiation and proton radiation [1]

Red color represents a large amount of radiation and light yellow represents a small amount of radiation. Considering the photon beam on the left of the Fig. 1.1, we see that normal tissue absorbs large amount of radiation and even larger than the tumor for some tissue. Thus new kind of radiation treatment is developed. Proton beam gives interesting results that the amount of radiation is specifically large at the tumor region and does not exist beyond the tumor. In this project, we are interested in depth dose distribution, where the dose is defined as energy deposited in medium per unit mass. The SI unit of dose is Gy (gray) or J/kg. From the comparison between depth dose distributions of photon and proton as shown in Fig. 1.2, we can see that proton can give highest dose at a target more precisely than photon. The peak of proton dose distribution has specific name known as “Bragg peak”.

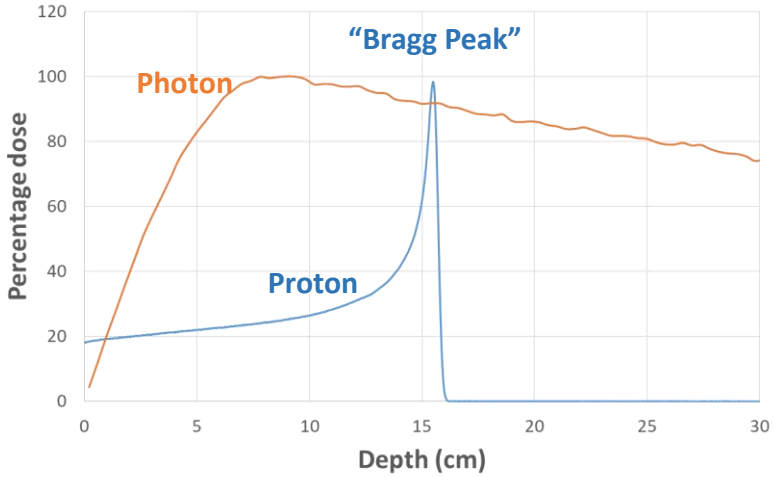

Fig. 1.2 Percentage depth dose distributions of photon (orange line) and proton (blue line)

In some cases, the tumor size is larger than the width of Bragg peak, therefore proton beam is needed to be modified to cover whole tumor size. This broaden peak is called “Spread-Out Bragg Peak” (SOBP) which is shown in Fig. 1.3.

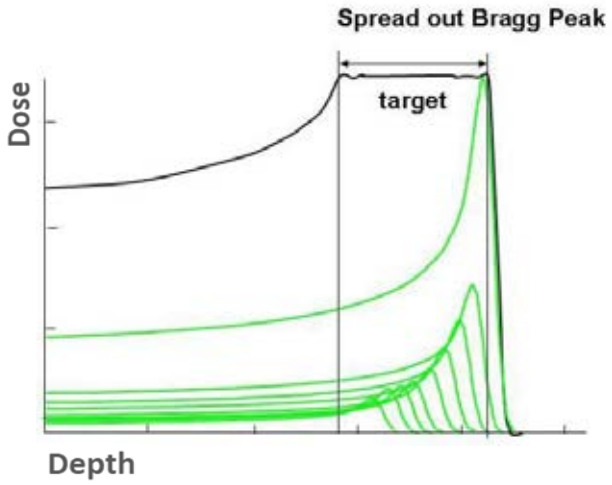

Fig. 1.3 Spread-out Bragg peak (SOBP)

Due to the special feature of proton energy deposition, the depth dose distribution of proton was studied in this project and compared with the depth dose distribution of photon. To get the depth dose distribution, two Monte Carlo transport simulation programs named PHITS and FLUKA were used and their results were also compared. We also generated SOBP from the modulation of proton depth dose distributions with various energies. First, we determined analytical calculation of proton depth dose distribution based on PHITS. Then, we used this calculation in the optimization program to determine initial energies and weighted intensities of proton beams which can generate SOBP covering target region in water.

The next chapter is theory, physics of proton and photon, related to the contribution of their depth dose distribution characteristics, are explained. The procedure and related physics, which implemented in these two simulation programs are described in chapter 3. Then, the description of methodology is in chapter 4 and the results are shown and discussed in chapter 5. Finally, chapter 6 is the conclusion.

Chapter 2

Theory

Due to different interactions of photon and proton with medium, their energy transfer characteristics are different. In this section, the related physical theory is described in order to explain the characteristic of the depth dose distribution of a photon and proton beam. First, we begin with photon interaction with matter. After that proton interaction with matter will be described.

2.1 Photon Interaction with Matter

Photon is an individual unit of energy. When a photon travels through a medium, it can interact with the medium in three possible ways: first, it can penetrate through matter without any interaction. Second, it can interact with the matter and be completely absorbed by depositing all of its energy by photoelectric effect, pair production, and photonuclear reaction. Lastly, it can interact and be scattered from its original direction and deposit part of its energy through Compton scattering.

2.1.1 Photoelectric Effect

In photoelectric process, an incident photon with energy $h\nu$ is absorbed by an atom. The photon disappears, and an electron is ejected from the atom. The electron emerges with kinetic energy ($T = h\nu - B$), where B is the binding energy of the electron in one of the states of the atomic shell (K, L, ...) from which it came. h is Planck's constant whose numerical value is 6.626176 x 10^{-34} J·s. After the inner electron is emitted, the outer electron will emit photon (x-ray) and occupy the state previously occupied by the emerged electron. If the electron of the medium absorbs this emitted photon and causes ionization along its path, it will be called "delta ray".

2.1.2 Compton Scattering

Compton scattering is different from photoelectric effect because it is the interaction between a photon and a valence electron. The energy of the photon is not entirely absorbed but is reduced as the photon is scattered. The wavelength of the scattered photon is related to its scattering angle (θ) as shown in Fig. 2.1 and can be determined by Eq. (2.1).

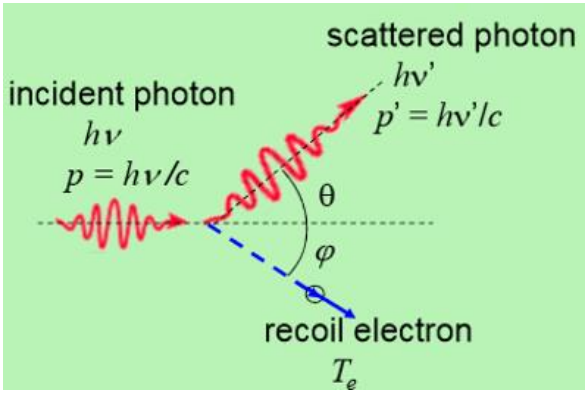

Fig. 2.1 Compton scattering [3]

$$\lambda' - \lambda = \frac{h}{m_e c}(1 - \cos\theta) \qquad (2.1)$$

λ' and λ are the wavelength of the scattered photon and the incident photon, respectively. m_e is electron mass and c is the speed of light. The energy which the recoil electron absorbs from the photon (ΔE) can be defined as

$$\Delta E = \frac{hc}{\lambda} - \frac{hc}{\lambda'} \qquad (2.2)$$

2.1.3 Pair Production

If photon energy is greater than twice of the rest mass of an electron (or 1.022 MeV) when the photon travels near the nucleus of an atom, the photon can interact with a virtual photon from Coulomb interaction with the nucleus by exchanging virtual electron. This interaction causes pair production of electron and positron sharing the energy of the disappeared photon.

2.1.4 Photonuclear Reaction

In this process, a photon interacts with a nucleus of the medium. The nucleus will absorb entire energy of the photon, and then emits a nucleon which is mostly neutron or it will be excited and then emits a gamma ray.

2.2 Attenuation of Photon

When photons enter into the medium, some of the photons encounter the four interactions described above and are absorbed or scattered. That means a photon can travel a certain distance before the interaction. The distance that a photon traveling in the medium without interaction depends on the probability of the interaction. In Fig. 2.2, mono-energetic photons enter into a uniform medium with adjustable thickness and may be detected by a photon detector behind the medium. Since the photon will either be absorbed or be scattered from its original direction after the interaction, thus the photon that is detected in the detector is the one which passes through the medium without interacting.

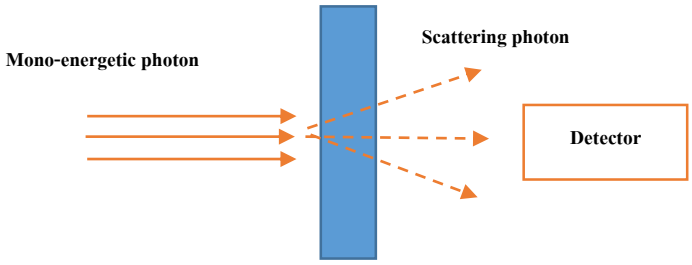

Fig. 2.2 The diagram of photon attenuation experiment

If a narrow beam of mono-energetic photons (N_0) enter a uniform medium, then the number $N(x)$ of the photons that can pass through the medium with thickness x without any interaction can be written as

$$N(x) = N_0 e^{-\mu x} \qquad (2.3)$$

where μ is a constant that is related to the probability of the photon interaction and depends on the energy of the photon and type of the medium. This constant is known as "linear attenuation coefficient" and an attenuation coefficient which is independent of the density of the medium is "mass attenuation coefficient", defined by dividing the linear attenuation coefficient by density of the medium (μ/ρ). From Eq. (2.3), the ratio the number of the photons that can pass through the medium of thickness x to the number of the incident photons is considered as the probability that the photon can pass through the medium of thickness x without interaction which is $e^{-\mu x}$. The attenuation of the photon is caused by the four interactions described previously. Since the probability of photonuclear reaction is very small compared to the others, therefore the attenuation coefficient consists of only three-terms of the three interactions.

$$\mu = \tau + \sigma + \kappa \tag{2.4}$$

where τ, σ and κ are attenuation coefficients of photoelectric effect, Compton scattering, and pair production, respectively.

2.2.1 Attenuation Coefficient of Photoelectric Effect

Attenuation coefficient of photoelectric effect (τ) depends on atomic number of the medium (Z) and energy of the photon (E) as shown in Eq. (2.5).

$$\tau \propto \frac{Z^n}{E^3} \tag{2.5}$$

n is a real number between 3 to 5 which depends on the energy of the photon. Eq. (2.5) shows that τ inversely depends on E^3, it suggests that photoelectric effect is important for photon with low energy.

2.2.2 Attenuation Coefficient of Compton Scattering

Attenuation coefficient of Compton scattering mainly depends on the number of electrons per the weight of the medium and slightly depends on the photon energy. Since the number of electrons per weight for each medium is nearly the same, this coefficient is nearly the same for various media.

2.2.3 Attenuation Coefficient of Pair Production

The probability of pair production depends on the energy of the photon and atomic number squared (Z^2). For a high energy region, this interaction dominates the attenuation of photon because the probability of photoelectric effect and Compton scattering decrease with increasing photon energy. For various media, the terms $\frac{(\kappa/\rho)}{Z^2}$ are nearly the same if the photon has the energy less than 20 MeV. In the case of the photon energy higher than 20 MeV, the probability of this interaction for a medium with higher atomic number is less than that for a medium with lower atomic number due to screening effect of atomic electrons.

2.2.4 Energy Transfer Coefficient and Energy Absorption Coefficient

Energy transfer coefficient (μ_{tr}) represents the probability that the energy of the photon is transferred to the medium at the interaction point, defined as the product of attenuation coefficient and the fraction of the mean energy transfer and the energy of the photon. In general, the energy transfer coefficient is equal to the energy absorption coefficient (μ_{en}). However, if there is radiation after the photon interaction, energy transfer is not equal to energy absorption but has a relation with μ_{tr} as

$$\mu_{en} = \mu_{tr}(1 - g) \qquad (2.6)$$

where g is the proportion of the energy that radiates from the interaction point. If we multiply the mass energy transfer coefficient by the energy of the interacting photon, we will receive a dosimetric quantity called kerma or kinetic energy released per unit mass. The SI unit of kerma is gray (Gy or J/kg), which is the same as the unit of absorbed dose. kerma is equal to absorbed dose only when the photon energy is low enough (e.g. 1 MeV). At this low energy, the range of electrons and positrons can be so short that the assumption of the kerma approximation is established. However, if the photon energy is rather high (a few MeV), kerma is not equal to absorbed dose because secondary charged particles do not deposit energies at the local interaction area.

2.3 Proton Interaction with Matter

The possible interactions of proton in the medium are inelastic scattering with an atomic electron, elastic scattering with a nucleus and nuclear reaction.

2.3.1 Inelastic Scattering with an Atomic Electron

In this process, a proton transfers a small amount of its energy to an electron without changing its direction because proton is much heavier than electron. Since a nucleus is very small compared to an atom, so the probability that the proton will be scattered off an atomic electron is greater than the probability that proton scatters off the nucleus. That means most protons will lose their small amount of energies continuously along their paths through the medium.

2.3.2 Elastic Scattering with a Nucleus

In this process, a proton is scattered off an atomic nucleus. Since the mass of most nuclei is much larger than the mass of proton except for light atom such as hydrogen, most protons are scattered off the nucleus and deflected from their original trajectories with unchanged kinetic energies.

2.3.3 Nuclear Reaction

Nuclear reaction can occur when a proton has sufficient energy to go through Coulomb barrier of a nucleus. The projectile proton enters and interacts with the nucleus; the nucleus may emit a proton, a deuteron, a triton, a heavier ion, or one or more neutrons. As a result, the number of primary protons of the beam is reduced in this process.

As mentioned above, protons are scattered off atomic electrons most frequent. Thus most protons lose their energies continuously as traveling through a medium. Next, we will consider energy loss rate of proton beam along the depth of medium and use it to describe the characteristic of proton depth dose distribution.

2.4 Stopping Power

Energy loss rate or stopping power is defined as the loss of kinetic energy E per unit path length.

$$S = -\frac{dE}{dx} \tag{2.7}$$

where S is the stopping power, E is the kinetic energy of the proton and x is the distance of proton traveling in the medium. For the average stopping power calculation, the method of SPAR coding, a FORTRAN program for computing stopping power and range, implemented in Particle and Heavy Ion Transport Code System (PHITS) [2], will be used. For this method, the stopping powers are computed using the continuous slowing-down approximation so that the energy loss fluctuation is neglected. The calculation of the

stopping power will be divided into three regions depending on the speed of the proton relative to the speed of light (β which can be defined in term of E as $\beta = \sqrt{\frac{(\frac{E}{m_p c^2}+1)^2-1}{(\frac{E}{m_p c^2}+1)^2}}$) and the nuclear charge number of the projectile particle (z) so in the case of proton z is 1.

- **Region I: $\beta > 0.04\, z^{2/3}$ or $E > 0.75$ MeV**

At this high energy region, a proton can be considered to completely interact with atomic electrons. The proton continuously loses its kinetic energy via inelastic Coulomb scattering with atomic electrons. Due to the high relative velocity between the proton and atomic electrons, atomic electrons will be considered as free stationary electrons. So the Bethe-Bloch's formula is used. The theory of Bethe-Bloch was initially developed by Bohr and was based on the calculation of the impulse of a stationary unbound electron and the impact parameter. Then a more accurate formula taken into account-quantum mechanical effects was developed by Bethe and Bloch. The stopping power of protons is defined as

$$S(E) = n\left[\frac{4\pi e^4}{m_e c^2}\right]\frac{{z_p*}^2}{\beta^2}\left\{\ln\left[\frac{2m_e c^2\beta^2}{(1-\beta^2)}\right] - \beta^2 - \ln\bar{I} - \overline{\left(\frac{C}{Z}\right)} - \frac{\bar{\delta}}{2}\right\} \qquad (2.8)$$

where

$S(E)$ is the stopping power of protons with kinetic energy (E)

n is the electron density of the medium

$m_e c^2$ is the rest energy of an electron

$\bar{I}$ is the ionization potential

Z_p^* is the effective charge number of proton (=1 for $\beta > 0.04$)

$m_p c^2$ is the rest energy of a proton

$\overline{\left(\frac{C}{Z}\right)}$ is the shell-effect correction

$\overline{Z}$ is the mean charge number of the nuclide in the medium

$\overline{\delta}$ is the density-effect correction

The quantities with bars indicate averages over all nuclide types in the medium.

- **Region II: $0.0046\, z^{1/3} < \beta \leq 0.04\, z^{2/3}$ or $10\ \text{keV} < E \leq 0.75\ \text{MeV}$**

In this intermediate energy region, charge reduction is important. Due to the slowing down proton, the effective charge of the proton becomes less than the nuclear charge because of electron capture. Therefore the stopping power in this region is still calculated from Eq. (2.8) but the effective charge number of the proton (z^*) has to be calculated from the empirical relation of Barkas [4],

$$z^* = z\left\{1 - \exp(-125\beta\, z^{-2/3})\right\} \qquad (2.9)$$

- **Region III: $\beta < 0.0046\, z^{1/3}$ or $E < 10\ \text{keV}$**

In this low energy region, both charge reduction and elastic scattering with nucleus are important. The theory of Lindhard *et al* [5] is used to calculate the stopping power. For electronic stopping power calculation, atomic electrons cannot be considered as free stationary electrons anymore because the velocity of proton becomes comparable or even less than the velocity of atomic electrons. The proton

can interact with many atomic electrons at the same time along its traveling path. The electronic stopping power is defined as

$$S^e = k\sqrt{E} \tag{2.10}$$

where k is determined from S (calculated in region II) at the boundary condition $\beta = 0.0046\, z^{1/3}$.

The stopping power caused by the elastic scattering with nuclide will be called the nuclear Coulomb stopping power and defined as

$$S_j^n = \frac{\left(\frac{A_j N_j}{N_a}\right)\left(\frac{d\epsilon}{dx}\right)_j}{G_j} \tag{2.11}$$

where

$$\left(\frac{d\epsilon}{dx}\right)_j = 4.51\sqrt{\epsilon_j}\ \exp(-2.54\ \epsilon_j^{0.277})$$

$$\epsilon_j = F_j E$$

$$F_j = 3.255 \times 10^6 \frac{A_j/(A_j+m)}{z\, Z_j (z^{2/3}+Z_j^{2/3})^{1/2}}$$

$$G_j = 1.96 \times 10^{-6} \frac{A_j(A_j+m)(z^{2/3}+Z_j^{2/3})^{1/2}}{z\, Z_j m}$$

A_j, Z_j, and N_j are the mass, charge, and atom density, respectively, for the j^{th} nuclide in the medium, m is mass of a proton and N_a is Avogadro's number.

The total stopping power is

$$S = S^e + \sum_j S_j^n \tag{2.12}$$

The stopping power of proton in water is plotted against the energy as shown in Fig 2.3. The range of energy is 5 - 250 MeV which is in high energy region (region I). Fig. 2.3 shows that the stopping power decreases when the energy of proton increases. It decreases rapidly when the energy is less than about 40 MeV.

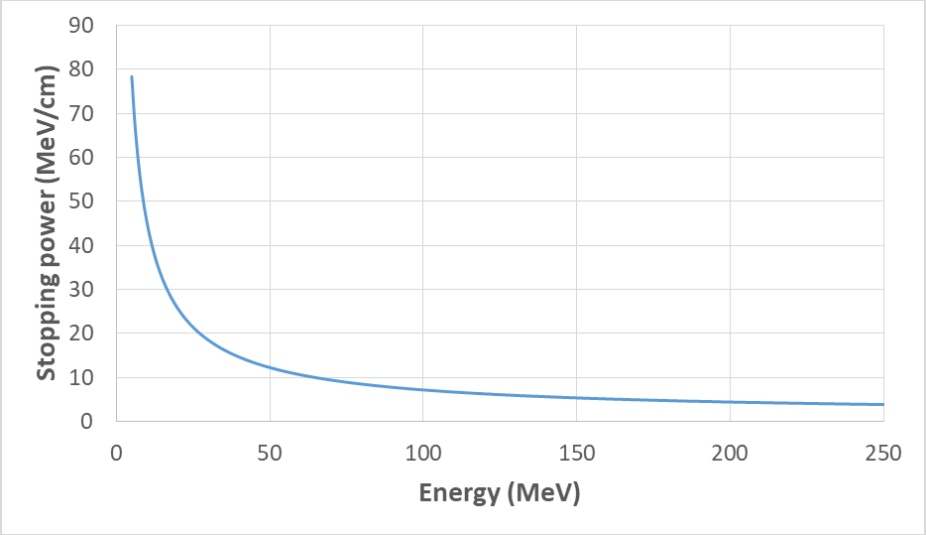

Fig. 2.3 The plot between stopping power of proton in water and the energy of proton between 5 – 250 MeV

2.5 Energy Straggling and Range Straggling

In the previous section, the calculation of the mean stopping power without considering the fluctuation of protons energy has been discussed. While each proton travels through the medium, it interacts differently along its path and causes small variation of its energy loss. The accumulation of this small energy loss variation affects the shape of proton dose distribution which will be explained later in chapter 5 (results and discussions). In Fig. 2.4, the energy loss distributions for various thicknesses of water are shown. Energy loss Probability Density Functions (PDFs that the protons lose an amount of energy (Δ) when

traveling through a water layer) multiplied by mean energy loss in the entire water thickness is plotted against the single event energy loss expressed as a fraction of the mean energy loss. $F(\Delta)$ is PDFs that the protons lose an amount of energy (Δ). Δ_{av} is mean energy loss in the entire water thickness and $(\Delta - \Delta_{av})/\Delta_{av}$ is a fraction of the mean energy loss. Fig. 2.4 shows the energy loss PDFs for various thicknesses of water, expressed in a unit of a mean free path (mfp). For thin absorbers (curves a–e, 256-4096 mfp), the PDFs are broad and asymmetric, and can be modeled with the Landau and Vavilov theories [6]. For thick absorber (curve f, 8192 mfp), the PDFs is symmetric (Gaussian distribution) and can be approximated with Bohr's theory.

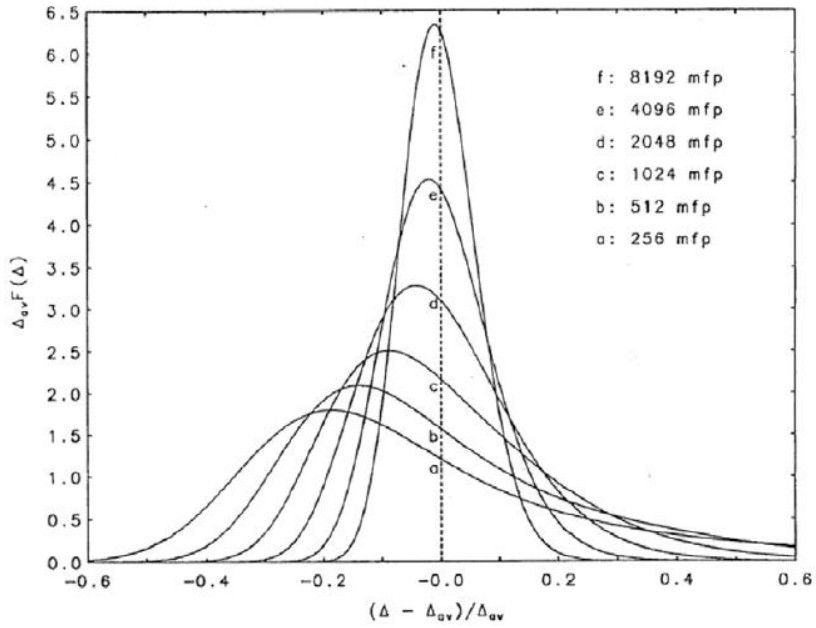

Fig. 2.4 The energy loss PDFs for various thicknesses of water in units of mean free path (mfp) [6]

Chapter 3

Simulation Procedure

In this section, the Monte Carlo particle transport code systems and optimization algorithm are described. We begin with the fundamental of Monte Carlo particle transport method and physical processes implemented in the program. Then the optimization algorithm will be described.

3.1 Monte Carlo Particle Transport Code Systems

Monte Carlo particle transport code system is a tool for calculation of particle transport and interaction with matter. There are two programs used in this project. The first program is Particle and Heavy-Ion Transport code System (PHITS) which has been developed under the collaboration among several institutes in Japan and Europe. The other is a fully integrated particle physics Monte Carlo simulation software (FLUKA) [7] which belongs to CERN and INFN. The similarity between these two programs is that they use Monte Carlo method for particle transport while the difference is physical models implemented in them.

Initially, a general algorithm of Monte Carlo simulation is explained. The simulation starts with the generation of a particle with a given position and momentum. If the particle is in a vacuum, it will be brought to the next material boundary. Total cross-section at

current energy is determined to obtain the mean free path of the particle. Then, the step length to the next interaction is sampled. The interaction is selected from all possible interactions according to their probabilities. Next, energy loss or scattering angle is sampled from differential cross-section for various interaction mechanisms. Note that these probabilities and cross-sections are from experiment. Then generated secondary particles are added. Finally, the process will be repeated until the particle energy is less than minimum cut-off energy or particle exits the geometry.

3.1.1 Physics in PHITS and FLUKA

Although the transport processes of both programs use Monte Carlo method, the physics models of them are different. In this section, we will discuss about the physical processes and physics models related to proton and photon interactions with matter.

3.1.1.1 Physics in PHITS

- **Physics of Proton in PHITS**

  The interactions between a proton and an atomic electron are the most frequent interactions. PHITS has used the SPAR coding, which is mentioned in section 2.4 to calculate the average stopping power of a proton without considering the energy loss fluctuation. For energy straggling, PHITS uses the Gaussian, Landau and Vavilov theories to deal with it. For the interaction between a nucleus and a proton with energy between 1 MeV and 3 GeV, the intra-nuclear cascade model (INCL4.6), and the generalized evaporation and fission model (GEM) are used.

- **Physics of Photon in PHITS**

In principle, a photon cannot deposit energy directly to matter, so there is no real "photon dose". On the other hand, secondary electrons generated by photoelectric effect, Compton scattering, and pair production can deposit their energies to matter. When the photon energy is low enough (e.g. 1 MeV), the range of secondary electrons generated from photon interaction can be so short that the assumption of the local approximation of the deposition energy is established. The calculated dose based on this local approximation (so-called kerma approximation) is generally called "photon dose". Then PHITS runs the simulation in photon transport mode using kerma approximation. However, if the photon energy is rather high (above a few MeV), Electron Gamma Shower5 (EGS5) mode is used to calculate electron and positron dose. For photonuclear reaction, hadronic cascade model named Jet AA Microscopic transport (JAM), quantum molecular dynamics named JAERI Quantum Molecular Dynamics (JQMD), and GEM are used.

3.1.1.2 Physics in FLUKA

- **Physics of Proton in FLUKA**

FLUKA treats the energy loss of proton calculation in 2 different treatments: small energy loss and large energy loss (large enough to cause delta ray). For large energy loss, energy loss is sampled from Mott cross-section for heavy ion [8]. For small energy loss, proton interacts with atomic electron thus there is more chance that proton will lose a small amount of energy. In this case, energy loss is not sampled

in an individual step. The mean energy loss can be calculated by Bethe-Bloch's formula as mentioned in Eq. (2.8) and taken into account of energy loss fluctuations. The detail of FLUKA's approach to energy loss fluctuations can be accessed in [7].

- **Physics of Photon in FLUKA**

In FLUKA, photon interactions are the same as PHITS. The secondary electrons and positrons doses are calculated as proton because they are both charged particles. The difference is that electron and positron dose calculations have to be taken into account the Bremsstrahlung effect. For photonuclear reaction, PreEquilibrium Approach to Nuclear Thermalization (PEANUT) is used.

3.2 Cut – Off Energy

Cut-off energies for certain types of particles used in PHITS [2] and FLUKA [7] are listed in Table 3.1 when we activated "negs mode" in PHITS and set the default to be in "precision mode" in FLUKA.

Table 3.1 Cut-off energy of PHITS and FLUKA

Type of Particle	**Cut-Off Energy of PHITS (MeV)**	**Cut-Off Energy of FLUKA (MeV)**
proton	1	0.1
neutron	1	10^{-11}
electron/positron	0.1	0.1
photon	0.001	0.1
deuteron, triton, and nuclei	1	0.1

others	2	0.1

3.3 Optimization without Constraint

In this project, the optimization method that we use is “steepest descent method”. This method is an iterative process that every step will lead to the variables with the lesser value of the function. Since gradient direction leads to variables with the larger value of the function as shown in Fig. 3.1. Red color represents the minimum value, purple color represents the maximum value of the function, and the arrows are gradient directions which pointing from red to purple. The length of arrow implies magnitude of the gradient. The magnitude of gradient is large when the length of arrow is long, and is small when the length of arrow is short. Therefore in every iteration, the variables will be changed in the direction of the negative gradient-direction to approach the minimum.

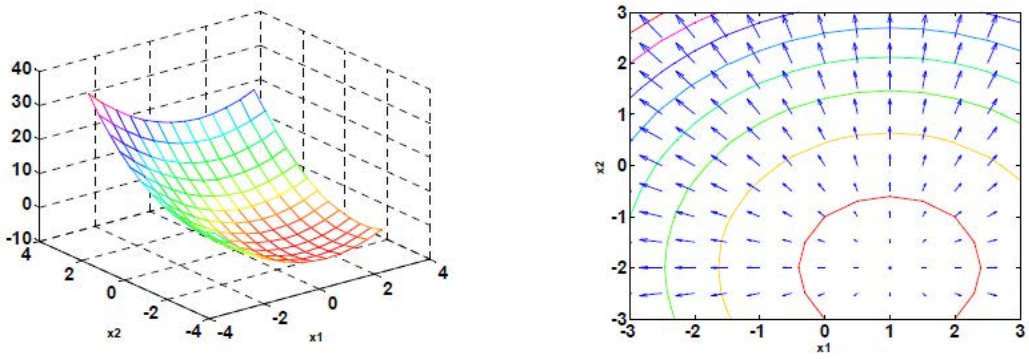

Fig. 3.1 The example function (left) and the direction of gradient of the function (right) [10]

$$x^{k+1} = x^k - \lambda^k \nabla^k f \tag{3.1}$$

Eq. (3.1) shows the adjustment of the variables (x^k) in each k^{th} iteration where $\nabla^k f$ is the gradient of the function (f) in k^{th} iteration. Next, the procedure of steepest descent is described.

1. Define initial variables x^0.

2. Calculate $\nabla^k f$.

3. Substitute x^0 and $\nabla^0 f$ in Eq. (3.1).

4. Calculate λ^0 which minimizes $f(x^1)$ then substitute λ^0 in Eq. (3.1) and get x^1.

5. Check whether $f(x^1)$ is less than $f(x^0)$ or not. If $f(x^1)$ is less than $f(x^0)$, then go back to step 2. If not, stop the process.

Chapter 4

Methodology

The methodology of this project consists of two parts: first, the study of depth dose distributions of mono-energetic photon beam and mono-energetic proton beam in various media using PHITS and FLUKA. Second, the modulation of mono-energetic proton beams to generate a spread-out Bragg peak (SOBP).

4.1 The Study of Depth Dose Distributions of Mono-Energetic Photon Beam and Mono-Energetic Proton Beam using PHITS and FLUKA

In this section, we simulated and compared the results of mono-energetic photon beam and mono-energetic proton beam traveling into cylindrical shaped media. The media that we used in this project are water, soft tissue, and compact bone. The depth dose distributions of photon and proton in water were generated by PHITS and FLUKA. Firstly, we determined the effects of initial beam energy and beam intensity on the depth dose distribution. Then, we determined mathematical function of proton depth dose distribution in water based on PHITS.

4.1.1 Generation of Depth Dose Distributions of Mono-Energetic Photon Beam and Mono-Energetic Proton Beam in Various Media using PHITS and FLUKA

The photon beam and proton beam are projected from the left end along the longitudinal axis of the cylindrical shaped media as shown in Fig. 4.1. The lengths of this cylindrical shaped media are set to be 40 cm and the radius is 10 cm. The beam width is set to be 7 mm by following the Full Width at Half Maximum (FWHM) at the skin surface of some facilities.

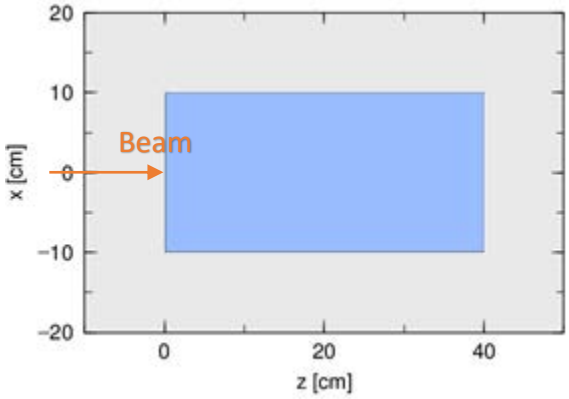

Fig. 4.1 The longitudinal section of the cylindrical shaped medium generated by PHITS

We used t-deposit tally function of PHITS and USRBIN scoring of FLUKA to determine the energy deposition in water discussed previously and provide the depth dose distribution data. Then, the results from these two programs were compared.

4.1.2 The Study of Depth Dose Distributions of Mono-Energetic Photon Beam and Mono-Energetic Proton Beam using PHITS and FLUKA

- **Determination of the Effect of Initial Energy on the Depth Dose Distribution of Photon in Water**

  We varied initial energies of photon beams to be 1, 5, 10, 15, 20, 50, and 150 MeV.

- **Determination of the Effect of Beam Intensity on the Depth Dose Distribution of Photon in Water**

  We varied beam intensities to be 2, 10, 50, 100, and 1000 photons while the initial energy of each beam is set to be the same value of 15 MeV.

- **Determination of the Effect of Initial Energy on the Depth Dose Distribution of Proton in Water**

  The initial energies of proton beams are varied to be 10, 75, 100, 125, 150, 175, 200, 225, and 250 MeV.

- **Determination of the Effect of Beam Intensity on the Depth Dose Distribution of Proton in Water**

  We varied beam intensities to be 2, 10, 50, 100, and 1000 protons while the initial energy of each beam is set to be the same value of 150 MeV.

- **The Depth Dose Distributions of Mono-Energetic Photon Beam and Mono-Energetic Proton Beam in Other Media**

In this section, we varied the beam energies of photon and proton to be the same as the case of water, but the medium is changed to be soft tissue and compact bone instead of water.

We set the material as soft tissue and compact bone according to the International Commission on Radiological Protection (ICRP) which provides values for density and mass fraction of certain medium as shown in Table 4.1.

Table 4.1 Densities and mass fractions of soft tissue and compact bone (ICPR)

	Soft Tissue	Compact Bone
Density (g/cm^3)	1.00	1.85
Mass Fraction		
Hydrogen	0.104472	0.047234
Nitrogen	0.02488	0.04199
Sodium	0.00113	-
Magnesium	0.00013	0.0022
Phosphorus	0.00133	0.10497
Carbon	0.23219	0.14433
Oxygen	0.630238	0.446096
Sulfur	0.0019	0.00315
Calcium	0.00023	0.20993
Chlorine	0.00134	-
Potassium	0.00199	-

Zinc	3×10^{-5}	-
Iron	5×10^{-5}	-

4.2 Determination of Mathematical Functions of Proton Depth Dose Distribution in Water based on PHITS

To get the depth dose distribution without running the simulation, we determined the mathematical functions by using PHITS. The characteristic of proton depth dose distribution in water was determined. The mathematical relation between the maximum dose and energy, and the relation between the dose at the surface of water and initial energy were fitted to obtain mathematical functions. Likewise, the relation between depths at certain percentages of the maximum dose and initial energies were determined. The depth at the maximum dose is denoted by R100, and the depths at 80%, 70%, 60%, 50, 40%, 35%, 30%, 10%, and 0.1% of the maximum dose are denoted by R80, L80, L70, L60, R50, L50, L40, L35, L30, R10, and R0.1, respectively. R or L is used to indicate the depths at each percentage either on the right or the left of the peak, respectively. For example, R80 means the depth at 80% of the maximum dose on the right of the peak. To complete the whole depth dose distribution, other unknown depths were determined from linear interpolation. Then, the depth dose distributions of proton with energies of 85, 110, 180, and 230 MeV obtained from mathematical functions were compared with the results from PHITS.

4.3 Modulation of Mono-Energetic Proton Beams to Generate Spread-Out Bragg Peak (SOBP)

SOBP is generated in order to make the modulated peak cover the target volume with a uniform dose. It can be calculated from the sum of various mono-energetic beams with appropriate beam intensities. In this section, we used the results from the study of the depth dose distribution of mono-energetic beam (section 4.2) to determine the energies of the beams whose peaks cover the target region and determine the weighted intensity of each beam that provides the uniform dose over the target region.

We wrote a program to determine the initial energy and the weighted intensity of each mono-energetic beam that satisfies the position of the target and a uniform dose over the target region. Figure 4.2 shows the input parameters and outputs of this program.

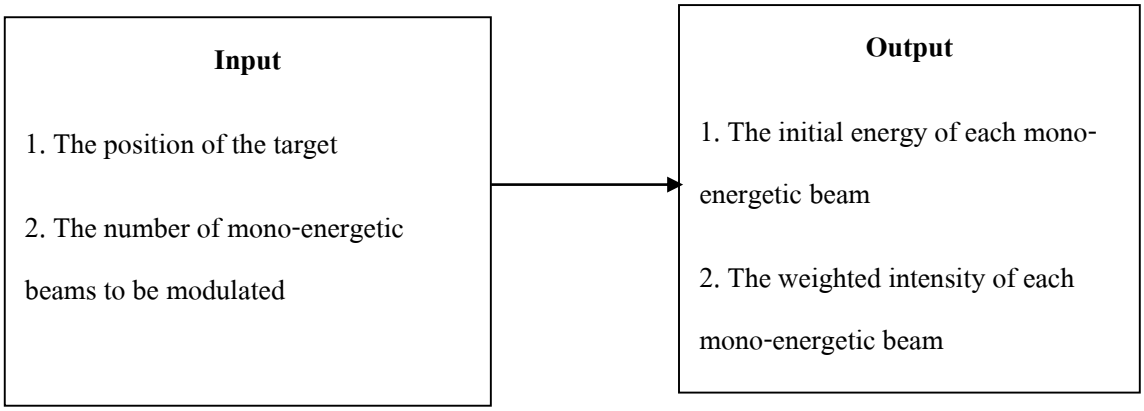

Fig. 4.2 The diagram shows the input parameters and outputs of the program.

In this program, the initial energy of each mono-energetic beam was determined from the relation between R100 and initial energy which is the result from section 4.2. First,

we determined the initial energies of the beams that cause the depth dose distributions peak at the edges of the target. Then the other initial energies that give peaks of the depth dose distributions between the edges of the target were determined.

Then, we determined the weighted intensity of each mono-energetic beam by optimization method. In this project, we used an optimization method called "steepest descent" whose its algorithm is described in chapter 3 (simulation procedure). In this project, the optimization function is

$$F(I_1, I_2, I_3, \dots, I_n) = \sum_{p=1}^{N-1} \sum_{r=p+1}^{n} (D_p - D_r)^2 \qquad (4.1)$$

where

$$D_p = \sum_{i=1}^{N} I_i D_{pi}$$

$F(I_1, I_2, I_3, \dots, I_n)$ is the optimization function which is the function depending on beam weighted intensity (I_i).

n is the number of beams from the input.

N is the number of points (positions) in water that is used to calculate the sum of dose.

I_i is the weighted intensity of the i^{th} beam.

D_{pi} is the dose of the i^{th} beam at the p^{th} point which is obtained from mathematical functions.

The program calculates I_i which minimizes the optimization function.

After we got initial energy and weighted intensity of each mono-energetic proton beam from the optimization program. We verified the results by using these beam parameters to generate SOBP in PHITS. In this study, the target is located at 6 - 8 cm from the skin surface of the water. The modulated-beam is generated from 4 and 10 mono-

energetic beams. To check the result in another region, we also generated SOBP from 10 beams, covering the target at 10 – 15 cm.

Chapter 5

Results and Discussions

In this chapter, we show the results and discussions following the procedure in methodology. First, the physics which contributes to the characteristic of the depth dose distributions of photon and proton is described. Then, the results of the variation of beam energies, beam intensities, and media are discussed. Finally, the SOBPs generated from modulation of mono-energetic proton beams are shown.

5.1 The Study of Depth Dose Distributions of Mono-Energetic Photon Beam and Mono-Energetic Proton Beam using PHITS and FLUKA

In section 5.1.1, we begin with the results of the effects of initial energy and beam intensity on the depth dose distributions of photon and proton in water. Then, the results of photon and proton in other media are discussed later. In section 5.1.2, the mathematical functions for generating proton depth dose distribution in water are shown. The depth dose distributions of proton with energies of 85, 110, 180, and 230 MeV which are the results from mathematical functions are compared with the results from PHITS.

5.1.1 The Study of the Depth Dose Distributions of Mono-Energetic Photon Beam and Mono-Energetic Proton Beam in Various Media using PHITS and FLUKA

- **Determination of the Effect of Initial Energy on the Depth Dose Distribution of Photon in Water**

To see the characteristic of the photon depth dose distribution, the percentage depth dose distributions are shown in Fig. 5.1. We will describe the depth dose distribution of photon by dividing into 2 parts: build-up part and decreasing part. The build-up part is the part where the dose increases up to the maximum dose. This increasing of the dose results from the accumulation of the number of the secondary particles (e.g. electron and positron) which are generated since photon has entered the water. For the decreasing part, due to attenuation of photons, the number of secondary particles is generated in lower rate. Therefore after reaching the maximum dose, the dose begins to decrease gradually. Fig. 5.1 also shows that the maximum dose locates deeper when the energies of photons increase. The reason is that high energy photon will transfer large amount of energy to secondary particles. It causes secondary particles being able to penetrate and deposit their energies further away from their birth place. It means that the secondary particles generated at the surface can travel and contribute to the maximum dose deeper in water when photon has higher energy.

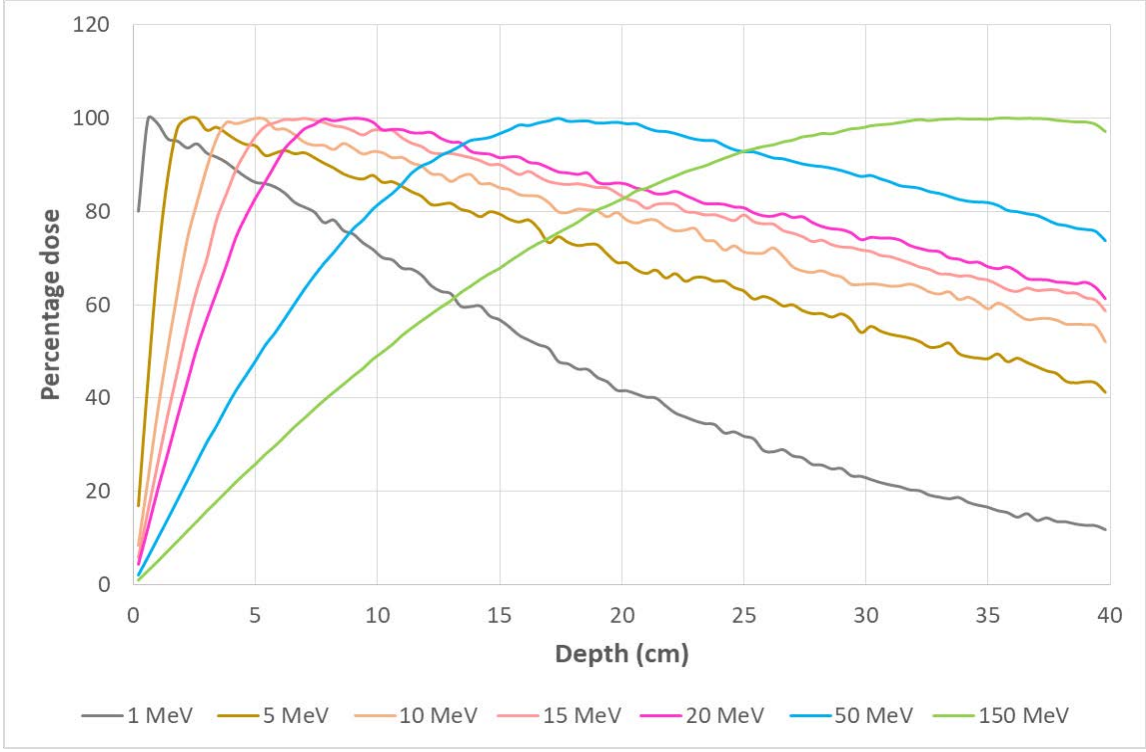

Fig. 5.1 Percentage depth dose distributions of photon with various energies in water

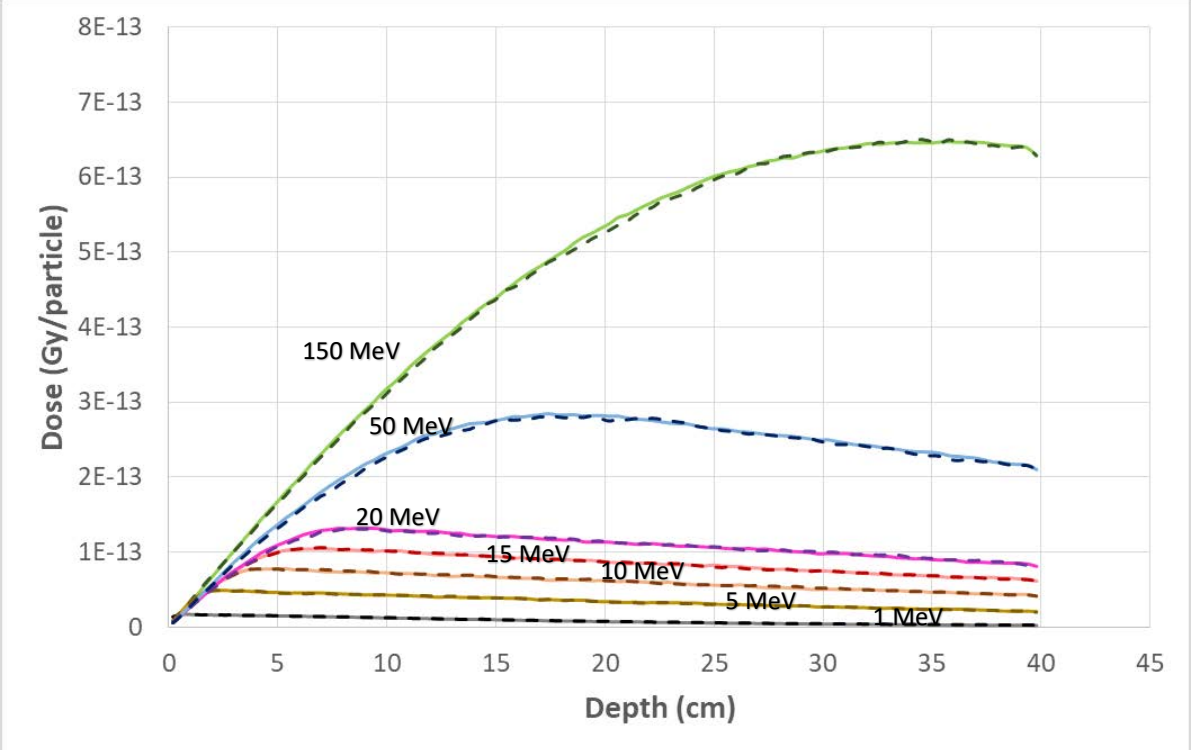

Fig. 5.2 The depth dose distributions of photon with various energies in water generated by FLUKA (dashed lines) and PHITS (solid lines)

Fig. 5.2 are the depth dose distributions of photon with energies 1, 5, 10, 15, 20, 50, and 150 MeV in water. Photon with higher energy deposits larger dose since high energy photon will deposit large amount of energy in water.

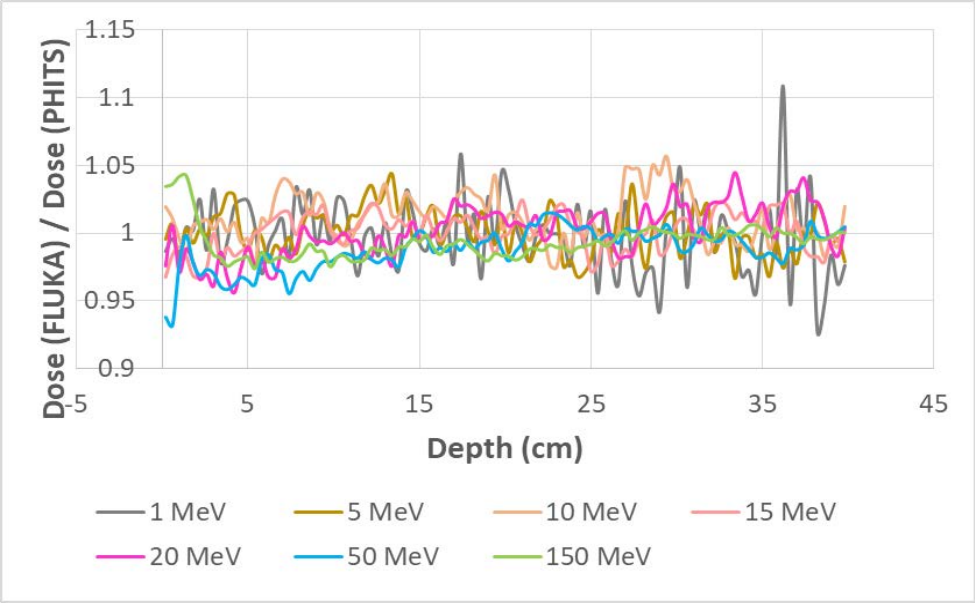

Fig. 5.3 The ratios of photon dose generated by FLUKA to the one generated by PHITS

Fig. 5.3 is the ratios of photon dose generated by FLUKA to the one generated by PHITS. The average difference between them is about 5% and the maximum difference is about 10%.

- **Determination of the Effect of Beam Intensity on the Depth Dose Distribution of Photon in Water**

We varied beam intensities to be 2, 10, 50, 100, and 1000 photons while the initial energy of each beam is set to be the same value of 15 MeV.

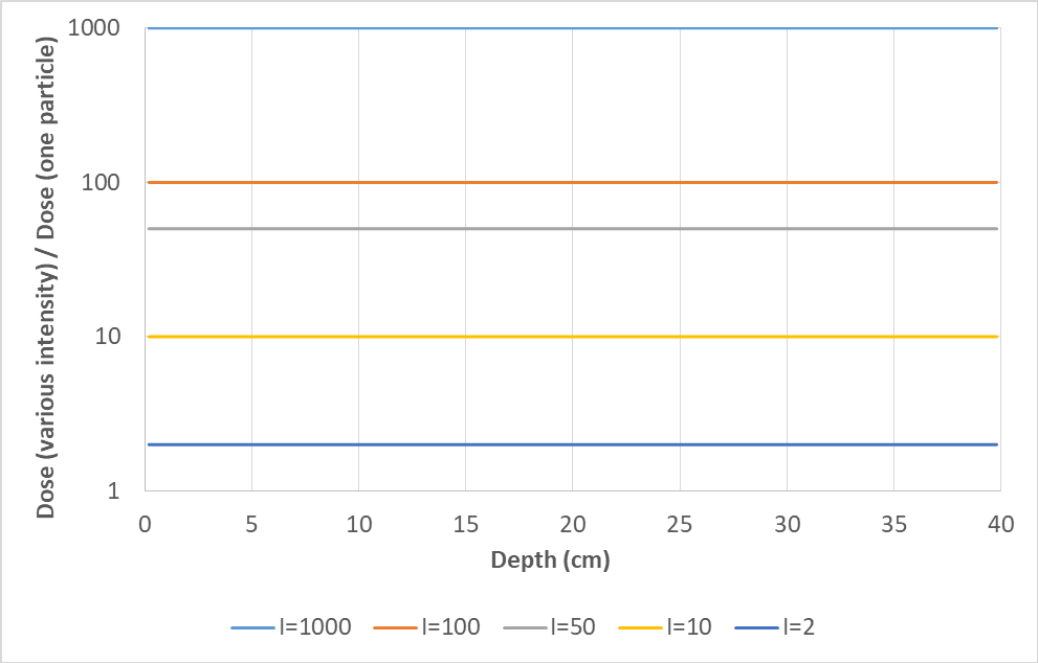

Fig. 5.4 The ratios of the dose of various intensities to the dose of one photon

Fig. 5.4 shows that, for the beam with N photons, its dose will be N times of the dose of one photon. Therefore, the dose is proportional to the number of photons or the beam intensity.

- **Determination of the Effect of Initial Energy on the Depth Dose Distribution of Proton in Water**

First, Fig. 5.5 and Fig. 5.6 are used to describe the physics behind the characteristic of proton depth dose distribution.

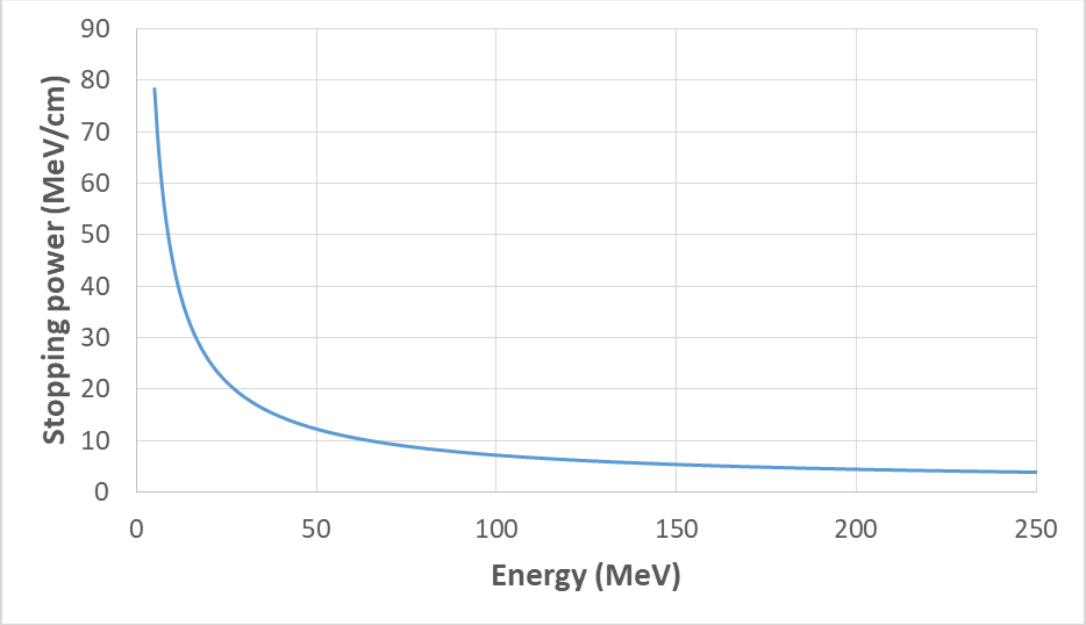

Fig. 5.5 The plot between stopping power of proton in water and the energies of proton between 5 – 250 MeV

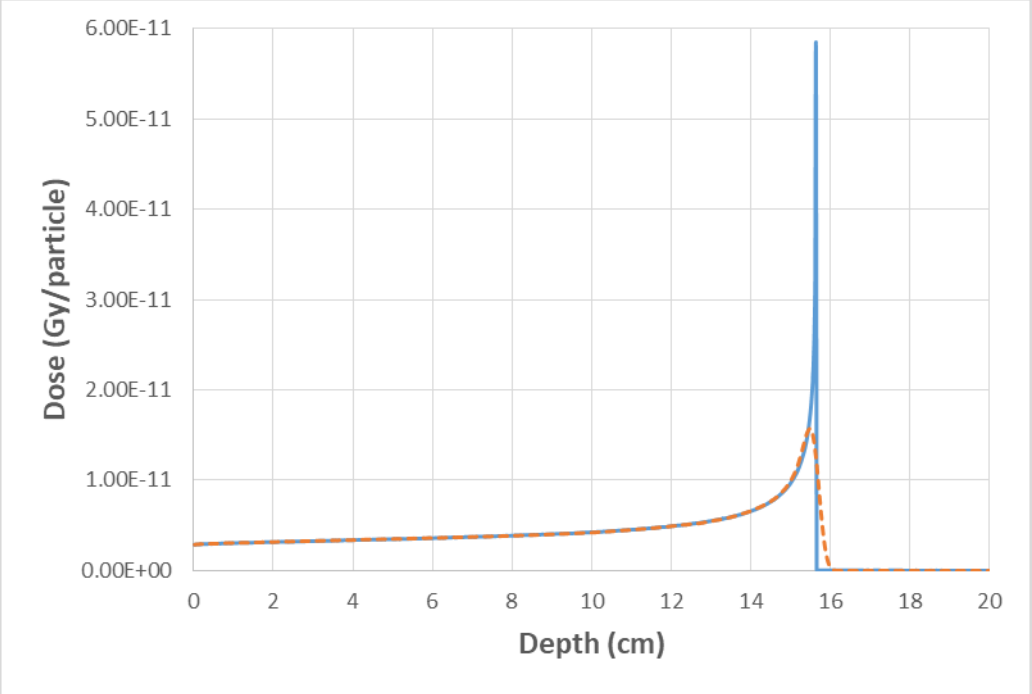

Fig. 5.6 The depth dose distributions of a proton with an initial energy of 150 MeV in water without considering energy straggling (solid line) and with considering energy straggling (dashed line)

Fig. 5.5 shows that the stopping power decreases when proton energy increases and decreases dramatically when proton energy is less than about 40 MeV. It means that a proton entering into the water with high initial energy will lose small amounts of its energy continuously and lose in higher rate when its energy is decreasing. The proton continues to slow down until its energy is about 40 MeV, according to Fig. 5.5, the stopping power increases rapidly. This causes proton to lose its large amounts of energy which contributes to the peak of the depth dose distribution known as "Bragg peak". Beyond the peak, the proton loses its entire energy and is absorbed by the water eventually. The solid line in Fig. 5.6 is the proton depth dose distribution which is simulated without considering the effect of energy loss fluctuation so the peak is very sharp. The accumulation of many small variations in energy loss causes energy straggling or range straggling (range is the distance that the proton travels through the medium until it stops traveling). The energy straggling consideration changes the shape of Bragg peak from solid line to dashed line which the peak is broader than the peak of solid line.

The depth dose distributions of proton with energies 10, 75, 100, 125, 150, 175, 200, 225, and 250 MeV in water are shown in Fig. 5.7.

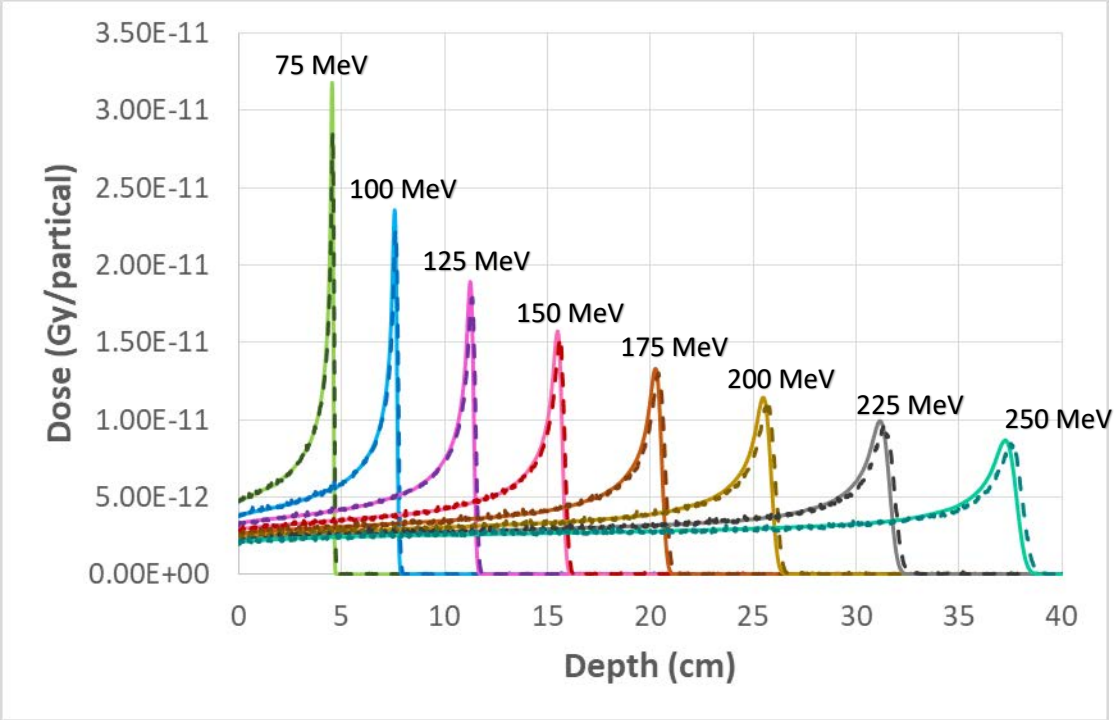

Fig. 5.7 The depth dose distributions of proton with various energies in water generated from PHITS (solid lines) and FLUKA (dashed lines)

Fig. 5.7 shows that proton with higher energies will be able to penetrate through water deeper than the lower one. The dose at the water surface for proton with lower energies is higher because low energy proton loses larger amount of energy according to Fig 5.5. The peak of high energy proton is broader because proton with higher energies travels through water deeper, causing more energy straggling. We also see that the depth dose distribution of proton with 10 MeV does not exist in Fig. 5.7 because the proton loses its entire energy since it is at the water surface.

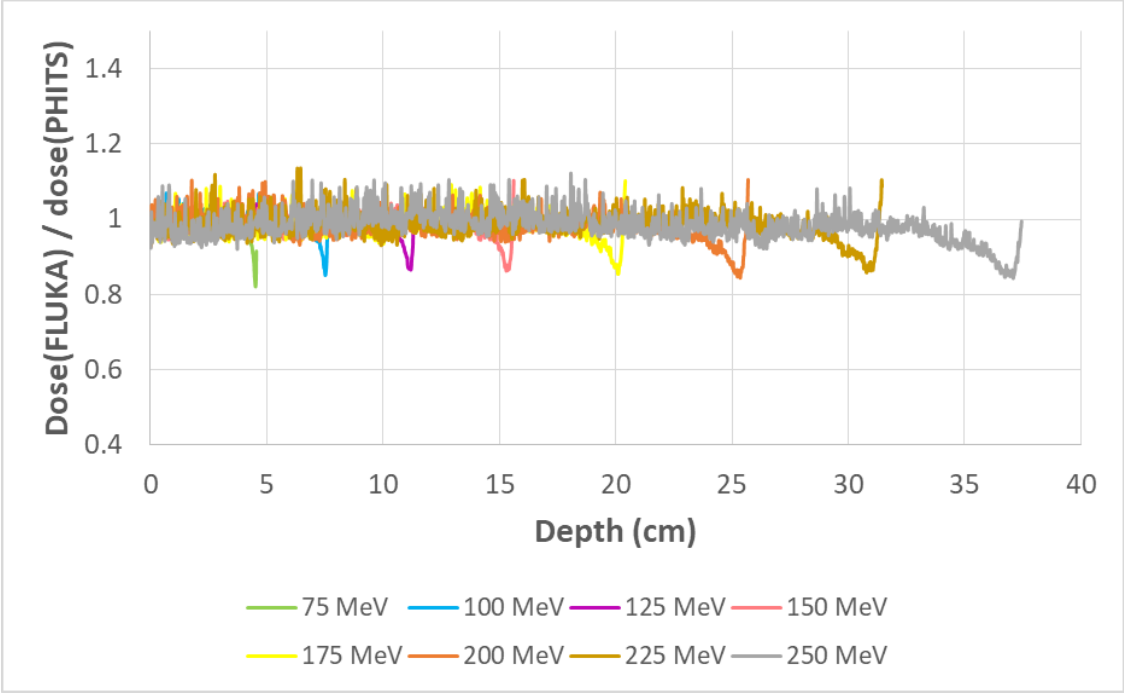

Fig. 5.8 The ratios of proton dose generated by FLUKA to the one generated by PHITS

Fig. 5.8 shows that the ratios of proton dose generated by FLUKA to the one generated by PHITS are about one, except for some depths near the peaks where the ratios change abruptly.

- **Determination of the Effect of Beam Intensity on the Depth Dose Distribution of Proton in Water**

We varied beam intensities to be 2, 10, 50, 100, and 1000 protons while the initial energy of each beam is set to be the same value of 150 MeV. The results show that doses of both photon and proton are proportional to the beam intensity.

- **The Depth Dose Distributions of Mono-Energetic Photon Beam and Mono-Energetic Proton Beam in Other Media**

In this section, the depth dose distributions of photon and proton in soft tissue and compact bone are compared with the results of water. We will discuss the results of photon first.

We will begin with the depth dose distributions of photon in soft tissue in Fig. 5.9b compared with photon in water in Fig. 5.9a. The results of every photon energies show that the doses and the depths of the maximum dose of photon in soft tissue are similar to that of water. The reason is that the density of tissue is 1 g/cm^3 which is equal to the density of water since the main composition of tissue is water. This is the reason why water can be used to represent human tissue.

Next, we consider the depth dose distributions of photon in compact bone in Fig. 5.9c. We see that the dose of photon in compact bone is higher than the dose in water or soft tissue. It is due to the density of compact bone is 1.85 g/cm^3 which is higher than that of water or soft tissue. It means that the probability of photon interaction increases, therefore the secondary particles are generated rapidly. It causes the depth of maximum dose closer to the surface than water or soft tissue.

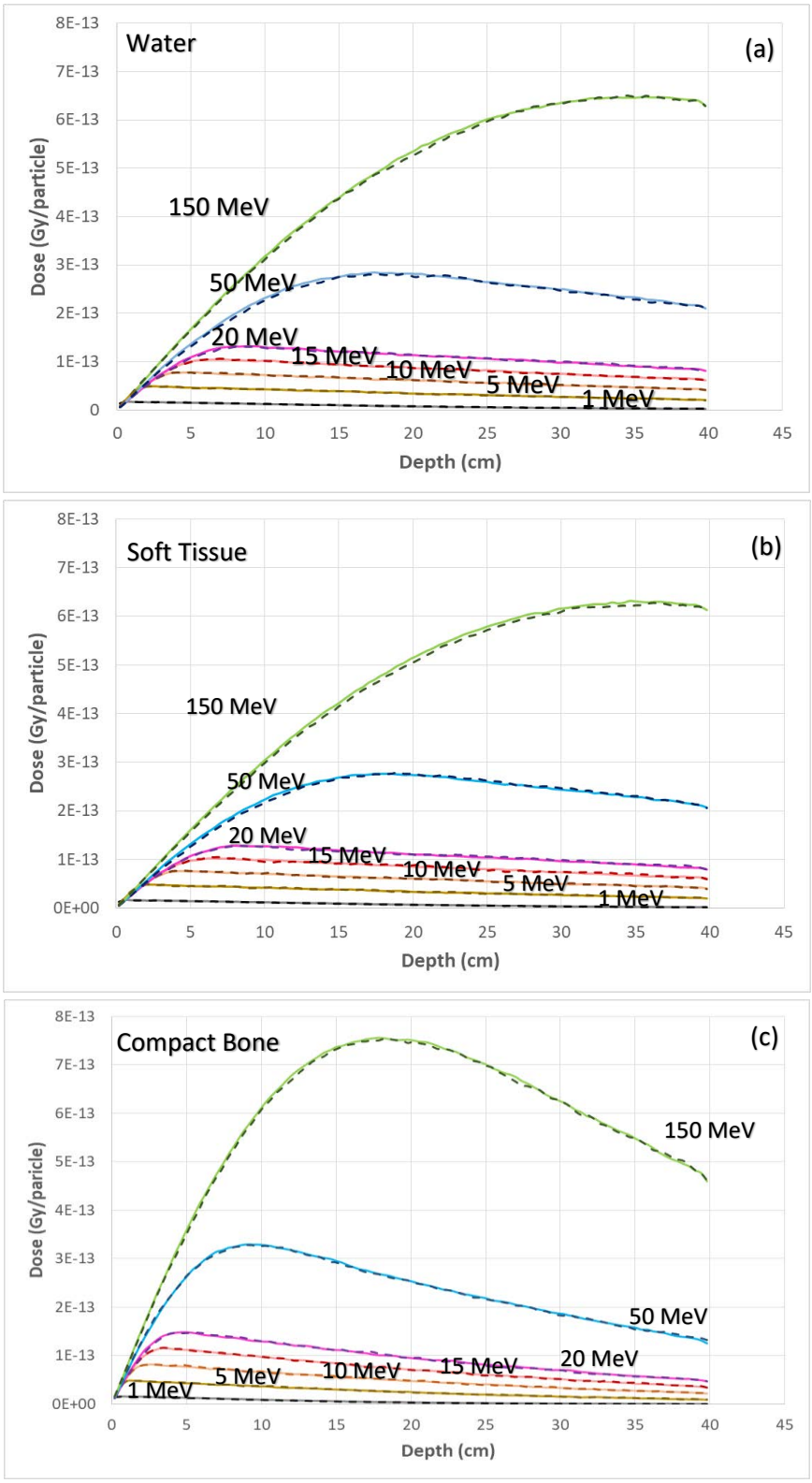

Fig. 5.9 The depth dose distributions of photon with various energies in water (a), soft tissue (b), and compact bone (c) generated by FLUKA (dashed lines) and PHITS (solid lines)

Next, the depth dose distributions of proton in soft tissue and compact bone are compared with the results of proton in water. Fig. 5.10 shows that the depth dose distributions of proton in soft tissue (Fig. 5.10b) are similar to the ones of water (Fig. 5.10a) since the properties of tissue and water are similar. For the depth dose distributions of proton in compact bone as shown in Fig. 5.9c, the ranges are shorter than the ranges of proton in water or soft tissue. Since compact bone density is higher than the density of water or soft tissue, the probability of proton interaction in compact bone is higher. This causes proton in compact bone losing its entire energy faster than proton traveling in water or soft tissue.

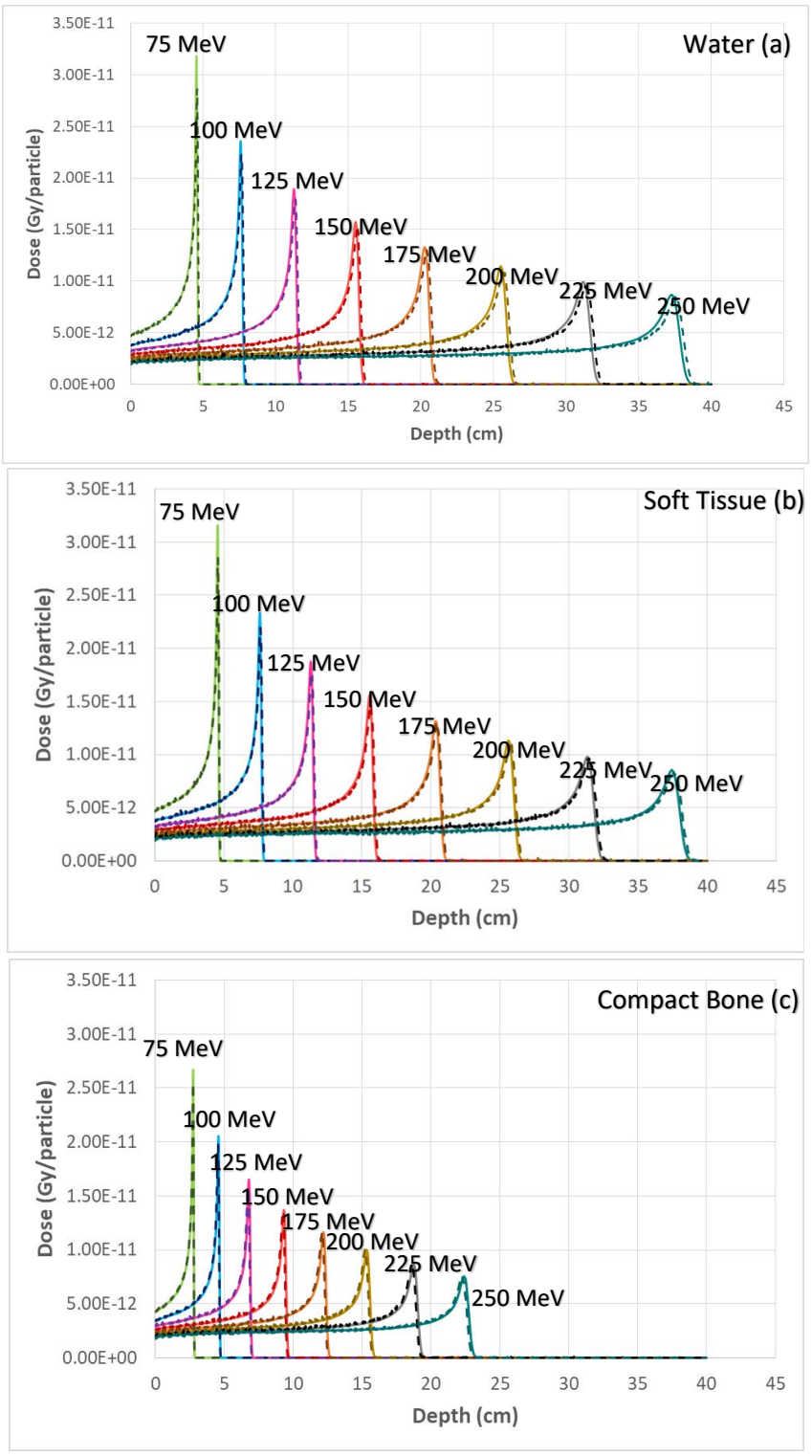

Fig. 5.10 The depth dose distributions of proton with various energies in water (a), soft tissue (b), and compact bone (c) generated from PHITS (solid lines) and FLUKA (dashed lines)

5.1.2 Determination of Mathematical Functions of Proton Depth Dose Distribution in Water based on PHITS

In this section, the results of the determination of the characteristic of proton depth dose distribution in water are discussed.

Fig. 5.11 shows the mathematical relation between the dose at the surface of water (D_s) and initial energy (orange dots) and the mathematical relation between the maximum dose (D_m) and initial energy (blue dots). The functions between the doses (e.g. the surface dose and the maximum dose) and initial energy are decreasing power function which are in the form of $D = AE^{-B}$, where D is the dose and E is initial energy. A and B are constants which range from 8×10^{-11} to 3×10^{-9} and from 0.674 to 1.071, respectively.

Fig. 5.12 shows the depth at the maximum dose which denoted by R100, and the depths at 80%, 70%, 60%, 50, 40%, 35%, 30%, 10%, and 0.1% of the maximum dose are denoted by R80, L80, L70, L60, R50, L50, L40, L35, L30, R10, and R0.1, respectively. R or L is used to indicate the depths at each percentage either on the right or the left of the peak, respectively. For example, R80 means the depth at 80% of the maximum dose on the right of the peak. The functions between the depths and initial energy are increasing power functions. The functions of the depths and initial energies are in the form of $R = CE^F$, where R is the depth and E is initial energy. C and F are constants which range from 0.0022 to 0.0035 and from 1.6155 to 1.7523, respectively.

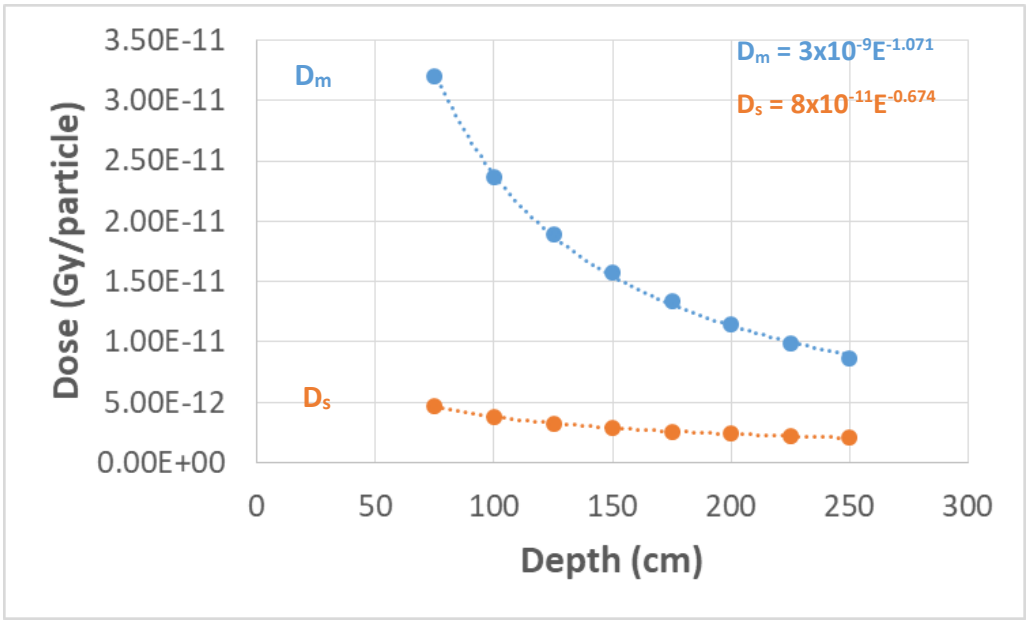

Fig. 5.11 The relation between the dose at the surface and initial energy (orange dots) and the relation between the maximum dose and initial energy (blue dots)

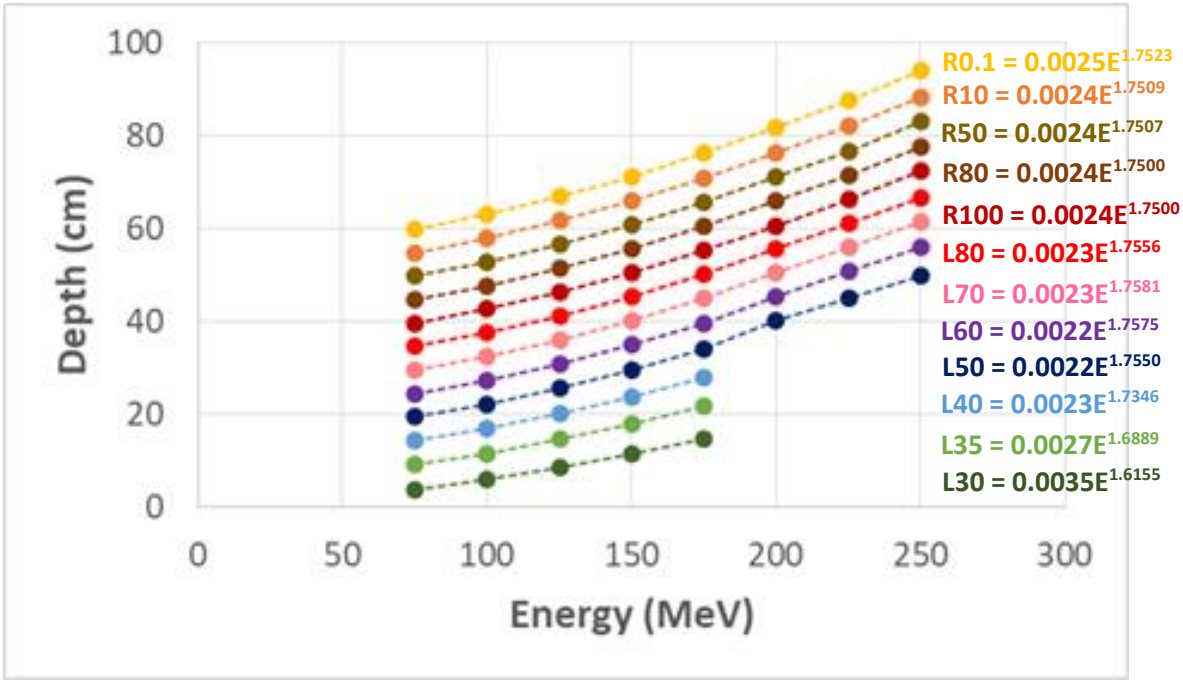

Fig. 5.12 The relations between the depths at 0.1% – 100% of the maximum dose and initial energy

Then the depth dose distributions of proton with energies of 85, 110,180, and 230 MeV (the energies that we did not use for fitting the graph) in water are determined using the mathematical functions obtained from Fig. 5.11 and Fig. 5.12. The other unknown points are determined by linear interpolation. Fig. 5.13 shows the comparison between the results from our mathematical functions (orange dots) and PHITS (solid lines). We can see that there is more inconsistency at higher beam energy.

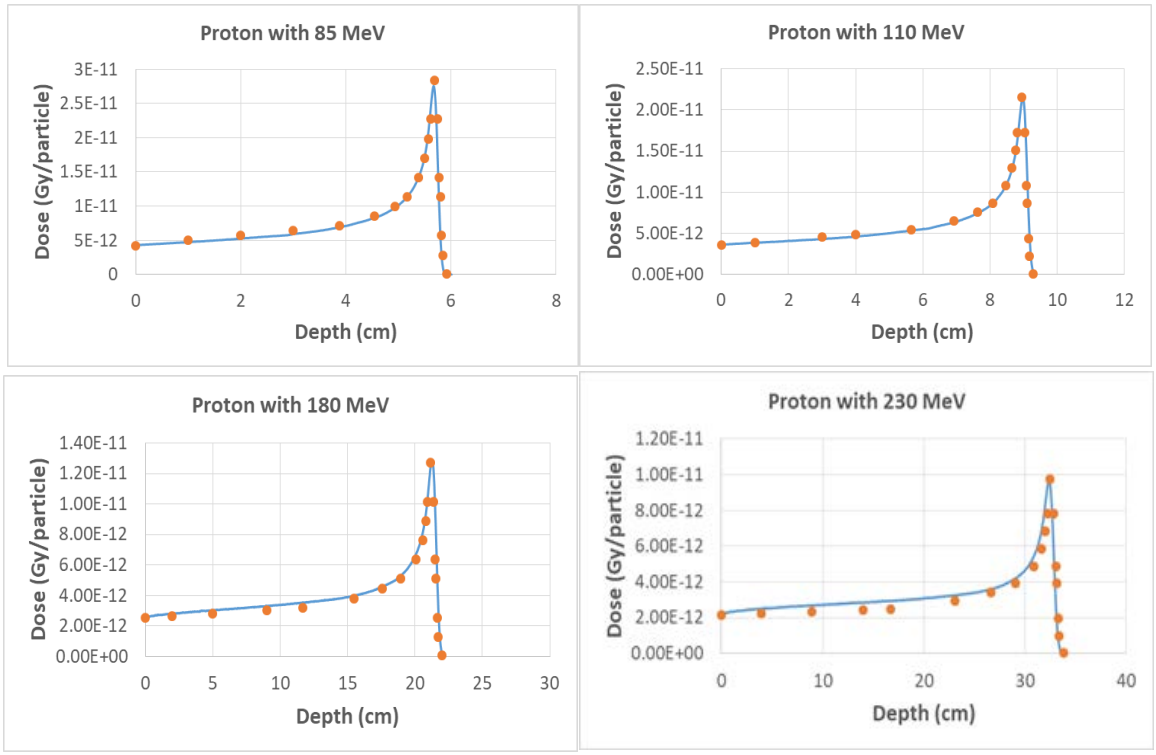

Fig 5.13 The depth dose distributions of proton with 85, 110,180, and 230 MeV in water from mathematical functions (orange dots) and PHITS (solid lines)

5.2 Modulation of Mono-Energetic Proton Beam to Generate Spread-Out Bragg Peak (SOBP)

In this section, we show some results of SOBP. This SOBP covers the region at 6 to 8 cm. The modulated-beam is generated from 4 mono-energetic beams with initial energies and weighted intensities determined from the optimization program. Table 5.1 shows the initial energies and weighted intensities which are the results of the program. We see that the weighted intensities are larger when initial energies are higher.

Table 5.1 The energies and the weighted intensities of 4 mono-energetic proton beams to generate SOBP covering at the region between 6 – 8 cm

Energy (MeV)	Weighted Intensity (I)
87.59	0.13
92.81	0.17
98.03	0.24
103.25	0.44

Fig. 5.14 shows the depth dose distributions of mono-energetic beams which will be used for the modulation to generate SOBP. The target locates at 6 – 8 cm which its boundaries are specified by the vertical red lines.

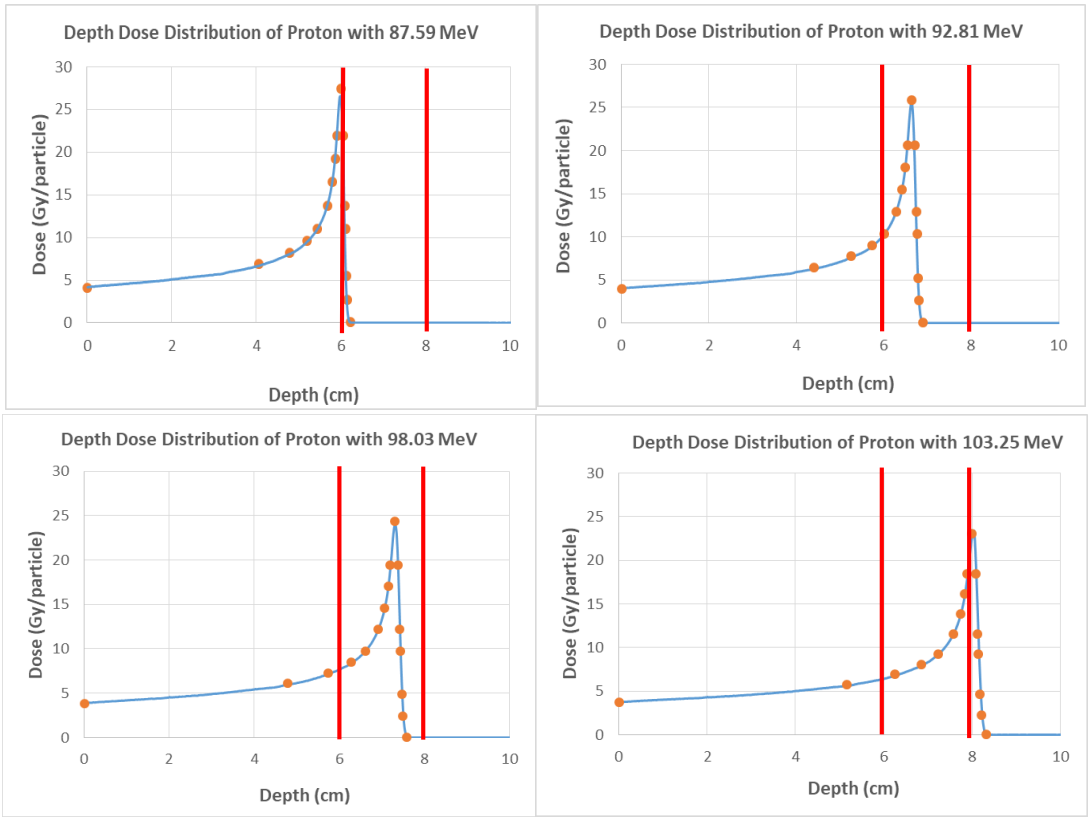

Fig. 5.14 The depth dose distributions of mono-energetic proton beams with the energies shown in Table 5.1 generated from mathematical functions (orange dots) and PHITS (solid lines)

Then we modulated all of the depth dose distributions in Fig. 5.14 with the weighted intensities in Table 5.1. The result of SOBP is shown in Fig. 5.15.

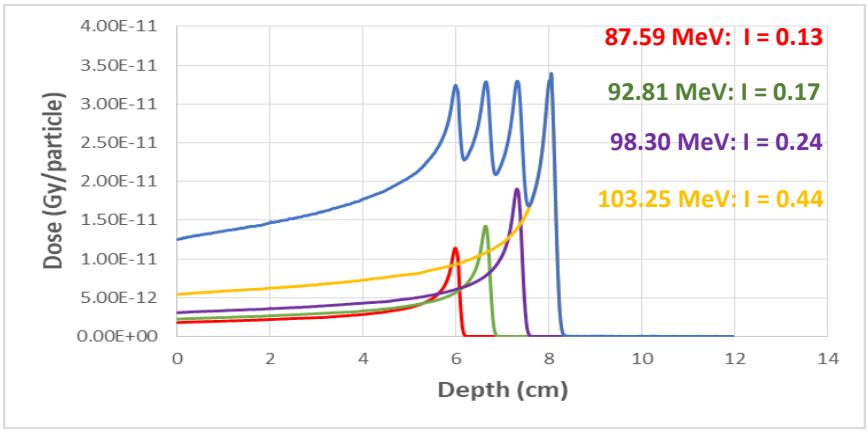

Fig. 5.15 The modulation of depth dose distributions from 4 mono-energetic beams with weighted intensities to generate SOBP (blue curve)

We see that using only 4 mono-energetic beams give 4 discrete peaks ranging from 6 - 8 cm. Next, we used 10 mono-energetic beams to generate more uniform SOBP covering the region at 6 - 8 cm. The result of the 10 mono-energetic beams modulation is shown in Table 5.2 and Fig. 5.16.

Table 5.2 The energies and the weighted intensities of 10 mono-energetic proton beams to generate SOBP covering the region between 6 – 8 cm

Energy (MeV)	Weighted Intensity (I)
87.59	0.03
89.33	0.04
91.07	0.04
92.81	0.05
94.55	0.06
96.29	0.07
98.03	0.08
99.7	0.10
101.51	0.14
103.25	0.38

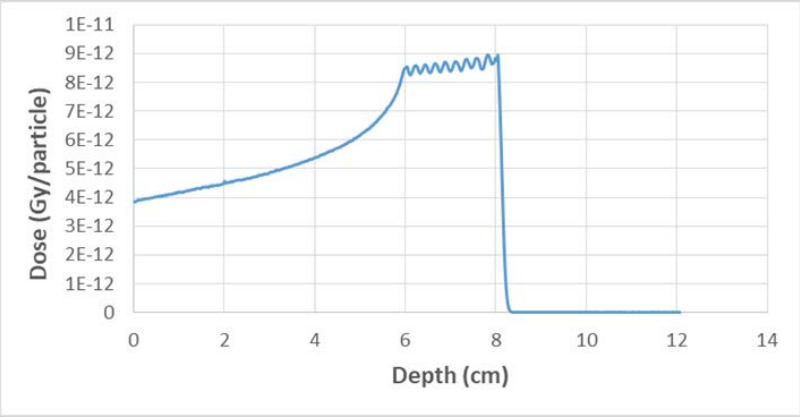

Fig 5.16 SOBP covering the region between 6 – 8 cm which generated from 10 mono-energetic beams

We see that SOBP in Fig. 5.16 has the value at the target region more uniform than the one of Fig. 5.15. To check the result in another region, we generated SOBP at the region between 10 – 15 cm. Table 5.3 shows the energies and the weighted intensities of 10 mono-energetic proton beams to generate SOBP covering the region between 10 – 15 cm.

Table 5.3 The energies and the weighted intensities of 10 mono-energetic proton beams to generate SOBP covering the region between 10 – 15 cm

Energy (MeV)	Weighted Intensity (I)
117.30	0.05
120.70	0.06
124.10	0.07
127.50	0.07
130.90	0.09
134.30	0.11
137.70	0.13
141.10	0.17
144.50	0.25

This is the result of the 10 mono-energetic beams modulation with the values in Table 5.3.

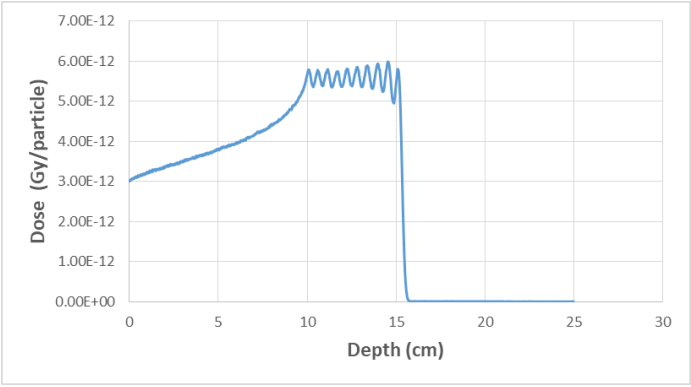

Fig. 5.17 SOBP covering the region between 10 – 15 cm which generated from 10 mono-energetic beams

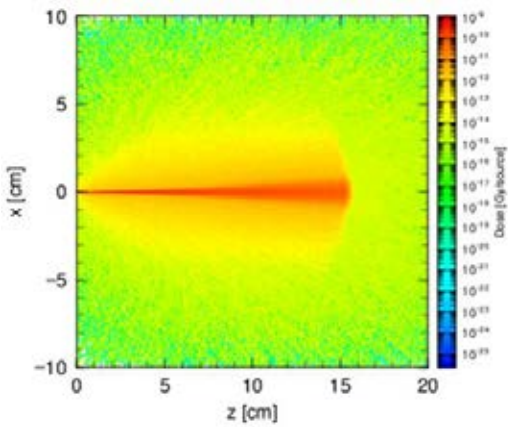

(a)

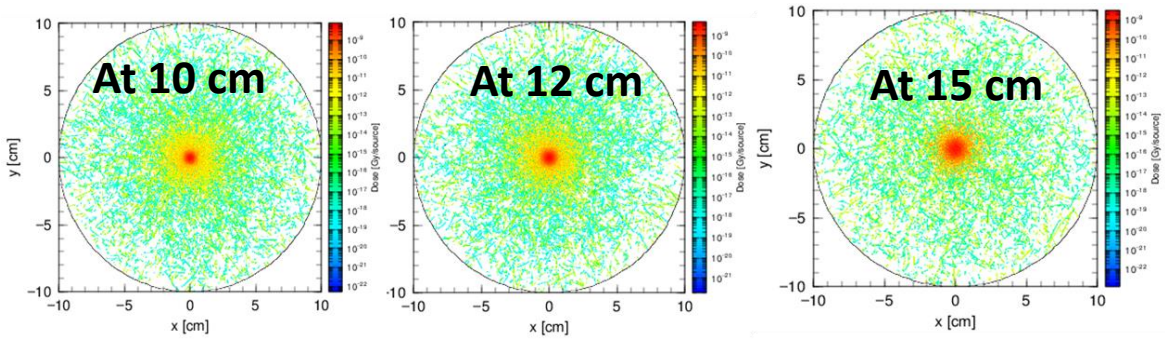

(b)

Fig. 5.18 SOBP covering the region between 10 – 15 cm. The dose in xz-plane (a) and in xy-plane (b)

Fig. 5.18 (a) shows that the beam width is narrow at the beginning and becomes broader at about the spread-out Bragg peak region. Fig. 5.18 (b) shows that the doses are symmetric around the *z*-axis. Thus in 3-dimensional treatment planning, the broader beam at high dose region have to be considered for sparing healthy tissue around the target.

Chapter 6

Conclusion

The depth dose distributions of photon and proton are completely different due to their different interactions with matter. The depth dose distributions of them depend on beam energy and beam intensity. For the effect of beam energy, when beam energy increases, the dose of photon increases while the dose of proton decreases. For higher beam energy, the depths at the maximum dose of both photon and proton are shifted to the deeper position in the medium. In the case of photon, the reason is that the secondary particles generated from photon interaction have more energy to travel and contribute to the maximum dose at deeper position of medium. In regard to proton, proton with high energy will lose small amounts of its energy according to Bethe-Bloch's formula which causes high energy proton to contain enough energy traveling to the deeper position of medium.

For the effect of beam intensity, the doses of both photon and proton are proportional to beam intensity. The depth dose distribution also depends on the type of medium. Soft tissue gives similar results to water but different from compact bone. The main cause is that the density of soft tissue is similar to that of water but different from compact bone. We also compared the results of PHITS and FLUKA which agree with each other.

Moreover, the characteristics of proton depth dose distribution in water were determined by using PHITS. The results show that the dose is a decreasing power function of initial energy while the depth at percentage of maximum dose is an increasing power

function of initial energy. These functions were used to reproduce the depth dose distributions of proton in water analytically. The results of our mathematical functions agree with the results of PHITS quite well. These depth dose distributions of proton were used in the optimization program to determine the energies and the weighted intensities of mono-energetic proton beams in order to generate SOBP to cover the target at 6 – 8 cm from water surface. The results of the optimization program reveal that the energies of modulated beams are 87.59 - 103.25 MeV. The weighted intensities are 0.13 – 0.44 for the modulation of 4 beams and 0.03 – 0.38 for 10 beams. It can be seen that the dose at the target region is quite uniform and is more uniform when more mono-energetic beams are used. For the additional work in the future, the broader beam at high energy region has to be considered to make three-dimensional SOBP which is more practical for cancer treatment planning.

References

[1] Sparing healthy tissue by leveraging the unique characteristics of protons. https://www.philips.co.uk/healthcare/education-resources/publications/hotspot/proton-planning. [Online; 4 September 2018].

[2] PHITS. https://phits.jaea.go.jp/rireki-manuale.html. [Online; 6 September 2018].

[3] Interactions of radiation with matter. https://humanhealth.iaea.org/HHW/MedicalPhysics/TheMedicalPhysicist/Studentscorner/HandbookforTeachersandStudents/Chapter_02.pdf. [Online; 2 November 2018].

[4] Walter H. Barkas, Nuclear Research Emulsions, Vol. 1, Academic Press, New York, 1963, p. 372.

[5] Armstrong, T. W., and K. C. Chandler. SPAR, a FORTRAN program for computing stopping powers and ranges for muons, charged pions, protons, and heavy ions. No. ORNL-4869. Oak Ridge National Lab., Tenn.(USA), 1973.

[6] Newhauser, Wayne D., and Rui Zhang. "The physics of proton therapy." Physics in Medicine & Biology 60.8 (2015): R155.

[7] FLUKA. http://www.fluka.org/fluka.php. [Online; 6 September 2018].

[8] Ionization and Transport. https://indico.cern.ch/event/694979/contributions/2927124/attachments/1657653/2654330/Ionization_and_Transport_2018.pdf. [Online; 6 September 2018].

[9] Fundamentals of Monte Carlo simulations of radiation transport with FLUKA.

https://indico.cern.ch/event/694979/contributions/2927088/attachments/1657637/2654305/Fundamentals_of_MC_simulations_of_radiation_transport_2018.pdf.
[Online; 6 September 2018].
[10] Unconstrained Multivariable Optimization.
http://inc.kmutt.ac.th/~yoodyui/courses/EEE603/slides/lecture4.pdf. [Online; 6 September 2018].
[11] Niita, Koji, et al. "PHITS—a particle and heavy ion transport code system." Radiation measurements 41.9-10 (2006): 1080-1090.